Hyperspectral Image Analysis for Iron Mineral Exploration and Spectral Unmixing Study in Kiriburu and Meghahataburu Mining Areas, West Singbhum, Jharkhand

Narayan Kayet[1], Khanindra Pathak[2,] Abhisek Chakrabarty[3] and Satiprasad Sahoo[4]

[1]Department of Remote Sensing & GIS, Vidyasagar University, Midnapore, INDIA
Email: narayankayet@gmail.com
[2]Department of Mining Engineering, Indian Institute of Technology, Kharagpur, Kharagpur -, INDIA
[3]Department of Remote Sensing & GIS, Vidyasagar University, Midnapore, INDIA
[4]School of Water Resources, Indian Institute of Technology Kharagpur, INDIA

Abstract

Key words: Hyperspectral remote sensing, Iron ores minerals, Linear spectral unmixing,

This paper contribution the results of the study to different iron ores minerals identification and their grade correction, using the hyperspectral imaging data in Kiriburu and Meghahataburu mining area. The study of EO-1 Hyperion data collection, pre processing of data (geometric, radiometric and atmospheric FLAASH correction), generated of spectral signature curves from the image for iron ore minerals, resampling the iron minerals image spectra and matching to USGS library spectra. Spectral inspections as a reference used in SAM technique to image classification for the identity of same iron ores minerals area calculated Hematite (36.7 %), Goethite (32.05 %), Limonite (5.04%) and Blue Dust (26.21%). The iron ores minerals classification overall accuracy 67 % and 0.6 kappa coefficient were calculated. Linear spectral unmixing (LSU) model was used for determining the relative abundance iron ore minerals. The optimum iron minerals abundances estimated by matching the computed mixed spectral signatures using the FWHM (Full width at half maximum) of High- Pass filtered method and standard error calculation. The sample -1 predicted the iron abundance of Hematite 70 %, Goethite 20 %, Limonite 5 %, Blue Dust 5% and standard error 0.00135. The sample- 2 predicted iron the abundance Goethite 75 %, Hematite 10 %, Limonite 10 %, Blue Bust 5% and standard error 0.000159. The sample- 3 iron predicted the abundance Limonite 55 %, Goethite 38 %, Limonite 5 %, Blue dust 2% and standard error 0.000973. The linear spectral unmixing method using in iron minerals abundance maps which, in conjunction with the image- and USGS laboratory-spectra, helped in assessing the grades of iron ores minerals in the study area. This analysis demonstrates the potential applicability of the methodology for iron minerals identification framework and discriminating grades of iron ores minerals.

1. Introduction:

A mineral is a naturally occurring chemical compound. Most often minerals are crystalline and abiogenic in origin. There are over 5,300 known mineral species; over 5,070 of these have been approved by the International Mineralogical Association (IMA). As per UNFC (The United Nations Framework Classification) system, India possesses the total hematite resources of 14,630 million ton of which 7,004 million ton are reserves, and 7,626 million ton are remaining resources. The major hematite resources are located mainly in Jharkhand-4036 million tons (28%), Orissa-4761 million tons (33%), Chattisgarh-2731 million tons (19%), Karnataka-1676 million tons (11%) and Goa-713 million tons (5%). The remaining balance resources are spread over the states of Maharashtra, Madhya Pradesh, Andhra Pradesh, Rajasthan, Uttar Pradesh and Assam and altogether contain around 4% of hematite. Jharkhand state is a land which blessed with the natural gift of immense mineral potential. The Jharkhand state is endowed with a rich deposit of Coal, Iron ore, Bauxite, Limestone, Copper, Mica, Graphite, and Uranium. Hematite (Fe2O3) which are confined to the Iron Ore Series of West Singhbhum district. This is richest in Asia also. It can be broadly divided into four sectors viz i) Noamundi ii) Kiriburu, Bara Jamda, iii) Gua, Ghatkuri, Karampada, iv) Kodlibad and Chiria- Manoharpur.

Hyperspectral remote sensing is very suitable for lithological discrimination which acquires reflectance or emittance data in many contiguous spectral bands such as for each pixel a complete spectrum can be derived from the covered wavelength region In particular, the 2.0–2.5- um shortwave infrared (SWIR) spectral range covers the spectral features of hydroxyl-bearing minerals, sulfates, and carbonates common to many geologic units and hydrothermal alteration assemblages. (Cloutis, E. A., 1996, Hubbard et al, 2005). The investigated alteration mineral mapping using ETM+ and Hyperion remote sensing data at Bau Gold Field, Sarawak, Malaysia the Landsat Enhanced Thematic Mapper + (ETM+) and Hyperion data were used to carry out mineral mapping of mineralized zones in the study area Directed Principal Components Analysis (DPCA) transformation of four appropriate ETM+ band ratios were applied to produce DPC images, which allow the removal of the effects of vegetation from ETM+ data and the detection of separate mineral images at a regional scale (Pour et al, 2014, Zadeh et al, 2014, Pour, A. B., & Hashim, M. (2013). Linear Spectral Unmixing (LAU) was used to produce image maps of hydroxyl-bearing minerals using Hyperion data at a district scale, which contains hydrothermally altered tertiary volcanic rocks. (Ducart et al, 2006, Boardman et al, 1995, Bierwirth, P. N., 1990). The Hyperspectral data were converted from radiance to apparent surface reflectance using radioactive transfer based on atmospheric modeling using a modified MODTRAN method. The data were than processed for mineral identification using SAM and Tricorder algorithm. The Tricorder uses an optimize least squared method

to compare the spectrum for each pixel on the scene to library spectra. (Crosta et al, 1998, Kruse et al, 1998, Bryant, R. G., 1996).The develops a new Extended Linear Mixing Model to address spectral variability. They developed the definition of an extended LMM (ELMM) to model spectral variability and shows that the use of spectral bundles models the ELMM implicitly. They also indicate that the constrained least squares (CLS) are an explicit modeling of the ELMM when the spectral variability is due to scaling effects (Veganzones et al., 2014, Drake, et al. 1999, Vaughan et all 2003). The experiments nonlinear hyper spectral Unmixing using Gaussian processes where they present an unsupervised algorithm for nonlinear unmixing of hyperspectral images. Where the proposed model assumes that the pixel reflectance result from a nonlinear function of the abundance vectors associated with the pure spectral components (Halima et al., 201l, Kayet, et al., 2015 and 2016, Sahoo et al., 2016).The used statistical method for deriving optimal spatial sampling schemes. Spectral angle mapper (SAM) and spectral feature fitting (SFF) classification techniques were applied to obtain rule mineral images. Each pixel in these rule images represents the similarity between the pixels in the hyperspectral image to a reference spectrum (P. Debba et al., 2005, Debba et al., 2005, Chen et al., 2007). The investigated has the effectiveness of EO1 Hyperion data acquired from the mined area for the discrimination of Iron ore in Keonjhar district, the northern part of Odisha, India. Using the parameters; the spectral classification is done by the spectral angle mapper classification (SAM) according to Spectral reduction by minimum noise fraction (MNF), spatial reduction by the pixel purity index (PPI) and manual identification of the end members using the N-Dimensional Visualizer (Mendoza, C., 2002, Sanjeevi et al., 2008).The used EO-1, Hyperion data has for the delineation of spatial variation of AL+OH minerals in a Part of Latehar and Gumla District, Jharkhand. They extract bauxites from Hyperion images by compensate for atmospheric effects using cross track illumination correction & the log residual calibration model and to validate result by MNF, PPI, SAM and Matched Filtering (Satpathy et al., 2010, Guha et al., 2013). The determines the Sub-Pixel Mineral Mapping Using Eo-1 Hyperion Hyperspectral data in the areas of the hostile mountainous terrain of Rajsamand district of Rajasthan; the study encompasses pre-processing, data reduction, PPI, and end member extraction from surface minerals such as illite, montmorillonite, phlogopite, dolomite, and chlorite. These endmembers were then assessed with USGS mineral spectral library and lab spectra of rock samples collected from the field for spectral inspection.(Kumar et al. 2014, Pour et al.,2014), The differentiate iron ores regarding their grades, using the hyperspectral (EO-1 Hyperion) image data, covering a mineralized belt in the Noamundi area, eastern India. They generation of spectral curves from the image for the iron ore deposits, extraction of the main spectral parameters and linear spectral unmixing for mapping iron ore abundance. Hyperion image pixels exhibit strong absorption at 850–900 nm and 2150–2250 nm wavelengths, which is typical of iron ores (Magendran et al., 2014, Gabr et al., 2010, Haest et al., 2013). The strength of the absorption features from the spectra varies according to the composition/grade of the iron ores and derived the Spectral parameters such as the depth, width, area and wavelength position of the absorption feature from the image spectra of that region and correlate well with the concentration of iron-oxide and alumina (gangue) in the ore samples obtained from the mine face. After that, the linear spectral Unmixing resulted in an iron ore abundance map which, in conjunction with the image- and laboratory spectra, helped in assessing the grades of iron ores in the study area

This paper contributes to the direction of the posterior facet of the research: i) Identify the iron ores minerals zones using Hyperion image ii) SAM algorithm is used to classify the pure pixel of Iron ores minerals iii) Estimation of the relative abundances of endmembers in a pixel using spectral unmixing method and standard error calculated. The proposed methodology is applied to Kiriburu and Meghahatuburu mining areas, Saranda Forest, Jharkhand,

2. Study Area:

Kiriburu and Meghahatuburu iron mining areas are the dense forest in the hilly region of West Singhbhum district in the Indian state of Jharkhand extends from latitude 22°00’45” -22°1’36” and longitude 85°08’18.8”- 85°24.37’21” and the forest covers an area of 820 km² (Figure-1).The average elevation of the Saranda forest is 755m. The name Saranda means seven hundred hills. Another origin of the name might be due to the presence of a vast number of elephant in the forest. Saranda also means Elephant. It is mining area including Gua, Chirriya, Kiriburu, Meghahatuburu, and Noamundi, etc. Kiriburu and its sister town Meghahatuburu both located in both Jharkhand and Odisha are one of the largest Hematite iron ore mines in the world. Mostly the forest is covered by the deciduous tree, and the dominant species of tree is Sal and Teak. Sal (Shorea robusta) is the most famous tree in the area, and it seems to have a preference for the rocky soil of the area.

3. Geological Setting:

The Older Metamorphics of Singhbhum region is believed to be the oldest rock exposed in the Jharkhand state constituting the basement of the Iron Ore Series. The rocks are represented by various types of Schists, Gneisses, Granulities, Quartzites, Meta basics and other essential intrusive and Granite. The famous “Singhbhum thrust zone” is the store house of several valuable minerals traversing East Singhbhum, West Singhbhum, and Saraikela-Kharsawan district as shown in Figure 1.This Singbhum Shear Zone (SSZ) Which is 1-10 km wide and 160 km long arcuate shaped belt separates the North Singhbhum Mobile Belt in the north from the Iron Ore Group and the Singhbhum Granite in the South. The area is an integral part of peninsular highland; that is part of Gondwanaland. Jharkhand state located in the Eastern part of India is a land blessed with the natural gift of immense mineral potential. The state holds a strong position on the minerals map of the country and is the store house of

more than 30 types of minerals possessing potential deposits of energy, ferrous, non- ferrous, industrial, fertilizer, refractory, atomaic, precious and non-precious group's minerals. Mostly the state is endowed with a large and rich deposit of Coal, Iron ore, Bauxite, Limestone, Copper, Mica, Graphite and Uranium.

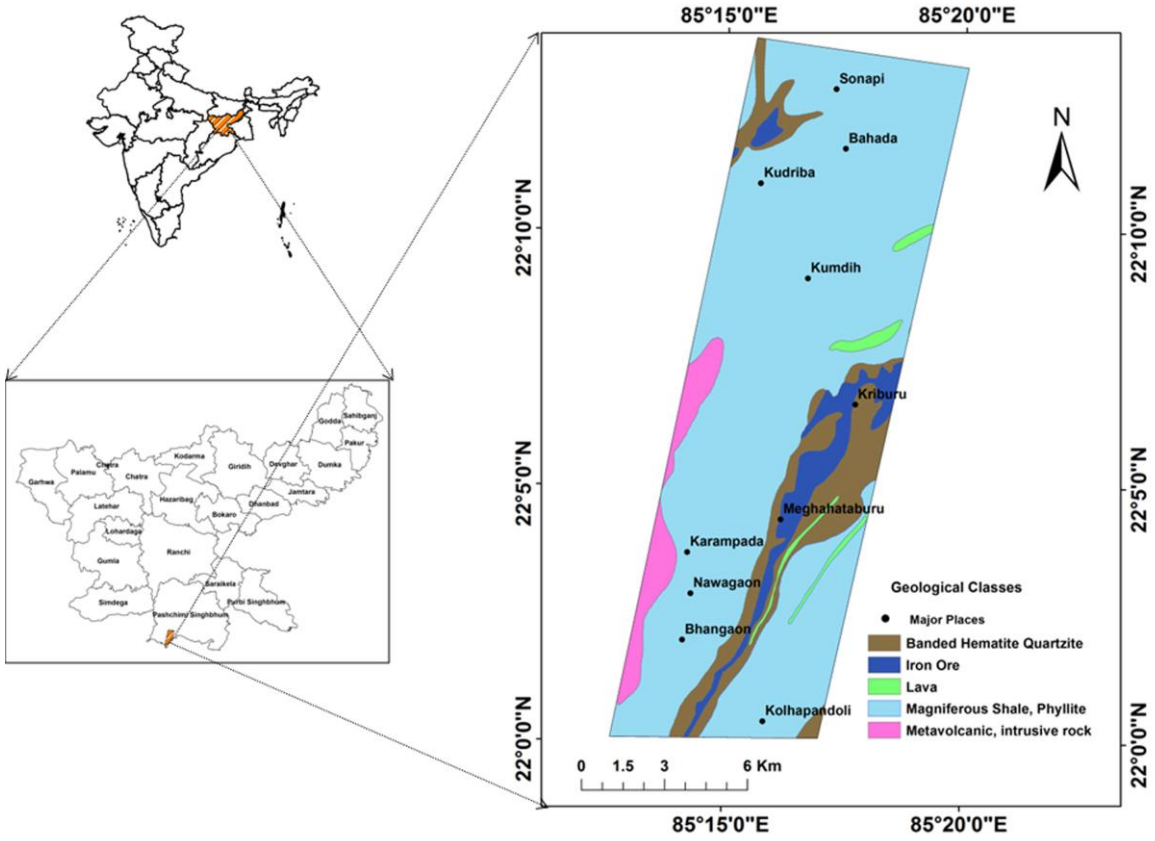

Figure :1 Location and geological map of the study area

4. Material and Methods:

4.1 Data used:

Hyperion is a hyperspectral instrument on the Earth-Observing 1 (EO-1) spacecraft that was launched from Vandenberg Air Force Base in the year November 21, 2000. The instrument payloads on the spacecraft are the Hyperion, ALI (Advanced Land Imager) and AC (atmospheric corrector). The primary objective of the Hyperion instrument is to provide high quality calibrated data that can support evaluation of hyperspectral technology for Earth observing missions. The Hyperion is a push broom imagine spectrometer; each image frame was taken in this "push broom" contains data for a 7.65 km wide (cross-track or perpendicular to the satellite motion) by185 km long (along-track) region and the image consists of 30 m x 30 m pixels. The 30 m size in the along-track direction was obtained by basing the frame rate on the velocity of the spacecraft for the 705 km orbit. Hyperion has a single telescope and two spectrometers, one is visible/near infrared (VNIR) spectrometer, and another is short-wave infrared (SWIR) spectrometer. The VNIR spectrometer uses a 70 (spectral) by 256 (spatial) pixel arrays, and the shortwave infrared (SWIR) spectrometer has 60 mm cooled Hgcdte detectors in an array of 172 (spectral) x 256 (spatial) channels which provides a 10 nm spectral bandwidth. Thus the dichroic filter in the system reflects the spectral region from 400 to 1,000 nm to a VNIR spectrometer and transmits the region from 900 to 2500 nm to a SWIR spectrometer. Geological map (Geological survey of India) and Toposheet Maps (Survey of India) were utilized for this purpose. GPS Survey and photographs are taken for collecting the ground truth data using the field verification.

4.2 Filed data collection:

The field surveys were carried out from Nov to Jan 2017. The 15 filed sample points of the gregarious different iron ore minerals, Hematite; Goethite, Desert, and Blue dust were recorded using DGPS (Differential Global Positioning System) field survey. The spectra for each iron ore minerals were recorded and averaged spectra used for the iron mineral mapping. Also, a total 130 ground control points with minimum 15 locations per iron minerals were collected following random sampling design to evaluate the iron mineral mapping accuracies.

4.3 Hyperspectral data pre-processing:

Hyperspectral remote sensing combines imaging and spectroscopy in a single system which often includes extensive data set and requires new processing methods. The Hyperion is a push-broom sensor with 242 contiguous and narrow bandwidth bands. A large number of bands provide the opportunity for more materials to be discriminated by their respective spectral response. However because of the huge volume of spectral data available, and the noise presents the space born hyper spectral data set, it requires careful pre-processing for managing the noise to reduce the complexity in analysis techniques. Several digital processing techniques are applied to remove geometric, radiometric and atmospheric distortions present in Hyperspectral images to extract meaningful information. The objective of pre-processing is to make remotely sensed data enable for efficient and reliable information extraction. The transformation of remotely sensed images so that it has a scale, projection system of a map is called the geometric correction. There are two types of error, i.e., internal geometric error and external geometric error. The internal geometric error is introduced by the remote sensing system itself or in combination with earth's rotation or curvature characteristics. The external geometric error introduced by the phenomena that vary in nature through space and time. The most external geometric error in remotely sensed data is random movements by aircraft at the exact time of data collection which includes altitude change, attitude change (roll, pitch, and yaw).Radiometric correction includes correcting the data for sensor irregularities and unwanted sensor or atmospheric noise and converting the data so that they accurately represent the reflected or emitted radiation measured by the sensor. All reflected and emitted radiations leaving earth's surface are attenuated mainly due to absorption and scattering by the constituents in the atmosphere; twice in case of reflection, once in case of emitted radiation. The electromagnetic signals recorded by space borne or airborne hyperspectral sensors are the combination of signals from the earth surface, atmospheric constituents and signal the error. Thus for the quantities analysis of the earth's reflectance, those atmospheric effects need to be removed from the acquired signals. The compensate for atmospheric effects, properties such as the amount of water vapor, distribution of aerosols, and scene visibility must be known because direct measurements of these atmospheric properties are rarely available, some techniques infer them from their imprint on hyperspectral radiance data. Atmospheric correction transformed the hyperspectral or multispectral data to apparent reflectance. Atmospheric correction is required for matching the image endmember spectra with the reference spectral libraries or ground truth. FLAASH is a physical base atmospheric mode for retrieving spectral reflectance from hyperspectral radiance images and was developed by spectral science under the sponsorship of the US Air force Research Laboratory. It compensates for atmospheric effect and corrects wavelength in the visible region. FLAASH has built support for hyperspectral sensors like Hyperion, AVIRS, HYDIC, HYMAP, and CASI For aerosol retrieval, FLAASH includes a method in which the aerosol amount and estimating a scene average visibility using a dark pixel reflectance ratio method based on work by Kaufman et al. (1997).The FLAASH currently interface with a pre release version of MODTRAN4. Thus the values of A, B, S, and La are determined from MODTRAN4 calculations that use the viewing and solar angles and the mean surface elevation of the measurement, and they assume a particular model atmosphere, aerosol type, and visible range. The values of A, B, S, and La are strongly dependent on the water vapor column amount, which is not well known and may vary across the scene.

4.4 Hyperspectral analysis:

The following method of Hyperspectral analysis was employed, as well as the MNF (Minimum Noise Fraction) transformation for reducing spectral data, the Pixel Purity Index (PPI) for identifying those last or spectrally pure pixels, and the n-dimensional visualizer for determining the endmember directly from the image. SAM was applied to estimate abundances of each endmember to produce final map.

4.4.1 Spectral angle mapper (SAM)

Spectral angle mapper is a supervised image classification process. A pixel with minimum spectral angle comparison with reference spectra is assigned to the pixel vector. A pixel with minimum spectral angle is the comparison to the true pixel is considering pure spectra of image spectrum. Monitoring the Earth using imaging spectrometers has necessitated more accurate analyses and new applications to remote sensing. With the increase in the high dimensional input, the hypothesis space grows exponentially, which makes the classification performance highly unreliable. New algorithms have to be developed for hyperspectral data classification.SAM is a physical based spectral classification method that computes the spectral similarity between an image spectra or test spectrum (t) and the reference spectrum (r) and is expressed regarding vector angle (Vander et al., 2006). This SAM algorithm used for pure pixel of Iron ores minerals mapping. For the SAM classification to be effective, the input image must be converted to apparent reflectance so that the data units are the same as the library units. SAM determines the similarity between an image spectrum (representing an unknown material) and a reference spectrum. (Representing a known material) by computing the spectral angle between them, treating them as vectors in n-dimensional spectral space, where n is the number of bands space. The angular differences between reference and target spectra are used for estimating the spectral similarity.

4.4.2 Spectral Unmixing:

Endmember variability has been identified as one of the main limitations of the usual Linear Mixing Model, conventionally used to perform spectral unmixing of hyperspectral data. A mixing model (linear or not) deals with; i) Estimation of the number

of endmembers to consider. ii) Extraction of the spectral signatures is of these endmembers. iii) Compotation of the corresponding relative is abundances. Many algorithms have been designed for this application. Most algorithms assume the signature mixing process of the pure materials and their proportions is linear. In case of multiple reflections of the light in its path from the ground to the sensor, or indirect lighting, or intimate mixtures, a good approximation may be achieved by nonlinear interactions. In this present study, linear mixing model of three endmembers using spectral signatures of Hematite, Goethite, and Limonite were attempted. The area also has a thin cover of blue dust. The abundance of blue dust has also been included in a residual component. The shape of the spectral profile is a major factor for matching spectral signatures. The most common spectra are a Gaussian profile. While specific spectrometer signatures are the well-defined theoretical band pass profiles. Noises in the optical system usually resemble the profile closer to a Gaussian shape. The width of the band pass is usually defined as the width in wavelength at the 50% response level of the function, called the Full Width at Half Maximum (FWHM).

4.4.3 Estimate Abundance of Endmembers in pixel:

Many algorithms have been designed for this application. Most algorithms assume the signature mixing process of the pure materials and their proportions is linear. In case of multiple reflections of the light in its path from the ground to the sensor, or indirect lighting, or intimate mixtures, a good approximation may be achieved by nonlinear interactions. Absorptions in a spectrum have two components: (1) continuum and (2) individual features. The continuum is the "background absorption" onto which other absorption features are superimposed. The depth of an absorption band, D, is usually defined relative to the continuum, Rc:

$$D=1-R_b/R_c$$

Where, Rb is the reflectance at the band bottom, and Rc is the reflectance of the continuum at the same wavelength as Rb (Clark and Roush, 1984).The depth of absorption is related to the abundance of the absorber and the grain size of the material. The concept of "band saturation" is the reflectance can never go to zero because of this reflection unless the index of refraction of the material is 1.0. The continuum-removal process isolates spectral features and puts them on a level. The strength of the iron absorptions depends on grain size. Larger grain sizes show (i) increased the saturation of the 0.9-µm absorption (ii) broadening and shifting the apparent reflectance minimum to longer wavelengths (Figure-2). The 0.9-µm absorption also shifts position with elements substituted for iron (e.g., see Morris et al., 1985). Continuum removal and scaling the hematite absorption to similar depth shows the wide variety of band shapes and positions that can be found in nature. For example, hematite has a narrower absorption at a slightly shorter wavelength than goethite. However, a coarse-grained hematite has a broader absorption, approaching the position and width of a fine-grained goethite (or a thin-film goethite).

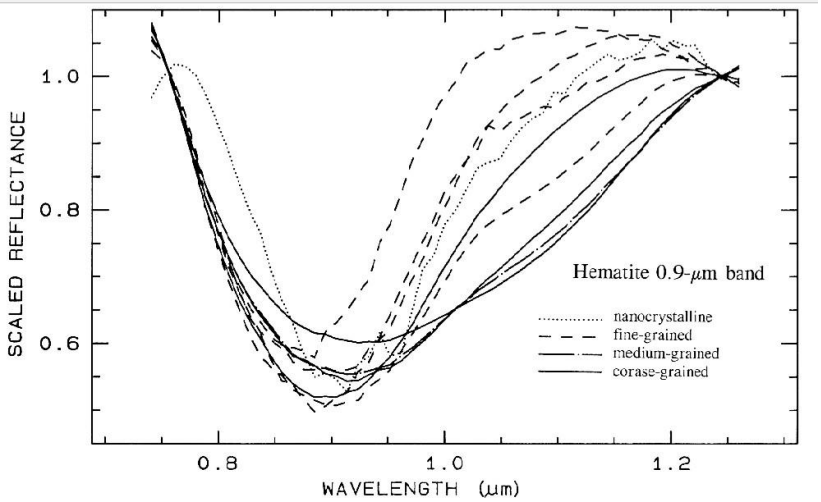

Figure: 2 Concept of absorption characteristics of different Minerals.

5. Results and Discussions:

5.1 Result of iron ore minerals:

The atmospherically corrected reflectance image was transformed MNF than PPI and n-dimension to collect the pure pixel of minerals .After that collection of different pure spectra from the open cast mines at different wavelength and save it to ASCII file or library files. A spectral resampling method was used to resample spectral data files to match the ASCII wavelength file. A spectral analyst method was used to analyst to help identify materials based on their spectral characteristics to match of an unknown spectrum to the materials in a spectral library. In the Kiriburu and Meghahataburu mines area there are four iron ore minerals could be identified viz; Hematite, Goethite, Limonite and Dust.

Hematite is the most important ore of iron (Fe2O3). It is a common rock forming mineral found in sedimentary, metamorphic, and igneous rocks at locations throughout the world. Hematite has a highly variable appearance; it always produces a reddish streak. Its lustercan range from earthy to sub metallic to metallic. Its color ranges include red to brown and black to gray to silver. It occurs in many forms that include micaceous, massive, crystalline, botryoidal, fibrous, oolitic, and others. Hematite is harder than pure iron, but much more brittle. Specific gravity is 4.9 to 5.3.

Goethite (FeO(OH) is an iron bearing hydroxide mineral of the diaspore group. It is found in soil and other low temperature environments. Goethite is an iron ox hydroxide containing ferric iron. It is the main component of rust and bog iron ore and its specific gravity varies from 3.3 to 4.3. Goethite often forms through the weathering of other iron rich minerals, and thus is a common component of soils, concentrated in laterite soils. The formation of goethite is marked by the oxidation state change of Fe2+ (ferrous) to Fe3+(ferric), which allows for goethite to exist at surface conditions and its color varies from Yellowish to reddish to dark brown or black.

Limonite is an iron ore consisting of a mixture of hydrated iron oxide hydroxides in varying composition FeO(OH)·nH2O. Most of limonite is made up of Goethite. Limonite is named from the Latin "limus" which means mud or in its yellowish lemon like color. In its brown form it is sometimes called brown hematite or brown iron ore. In its bright yellow form it is sometimes called lemon rock or yellow iron ore. Limonite is quite dense and hardness is within the range of 4 to 5.5, so somewhat lower than Magnetite and the specific gravity is between 2.9 and 4.3, The streak of limonite on an unglazed porcelain plate is always brownish, a character which distinguishes it from hematite with a red streak, or from magnetite with a black streak.

Blue Dust is a general term is observed in the form of steel blue coloured, fine to very fine grained, powdery Hematite with metallic luster and occurs in small exposure, having thickness of a few centimeters to meter where it takes the form of irregular pockets. It occurs association with BHJ and iron ore. The principles of iron bearing minerals of Blue dust are oxide (Hematite and Martite) and Hydroxide (Goethite). Below the following graph reflects the Hyperion image spectra of different iron ore minerals: The iron ores minerals spectral reflectance signatures and minerals map are showing in the figure 3.

Using physical based spectral classification method (SAM) developed by ENVIS, that computes the spectral similarity between the mineral spectra and reference spectra. In this algorithm the input image has been converted to apparent reflectance so that the data units are the same as the library units. After that the spectra of mineral has collected from the purest pixel of PPI image and then matched to the Spectral Library. The matched mineral spectra then analyzed with the Spectral Angle Mapper method to identify the different mineral classes. The aerial distribution of four mineral viz; Hematite, Goethite, Limonite and Dust has been covered at different compartment; where Hematite encompasses 36.7 %, Goethite 32.05 %, Limonite 5.04 % and dust 26.21 %.

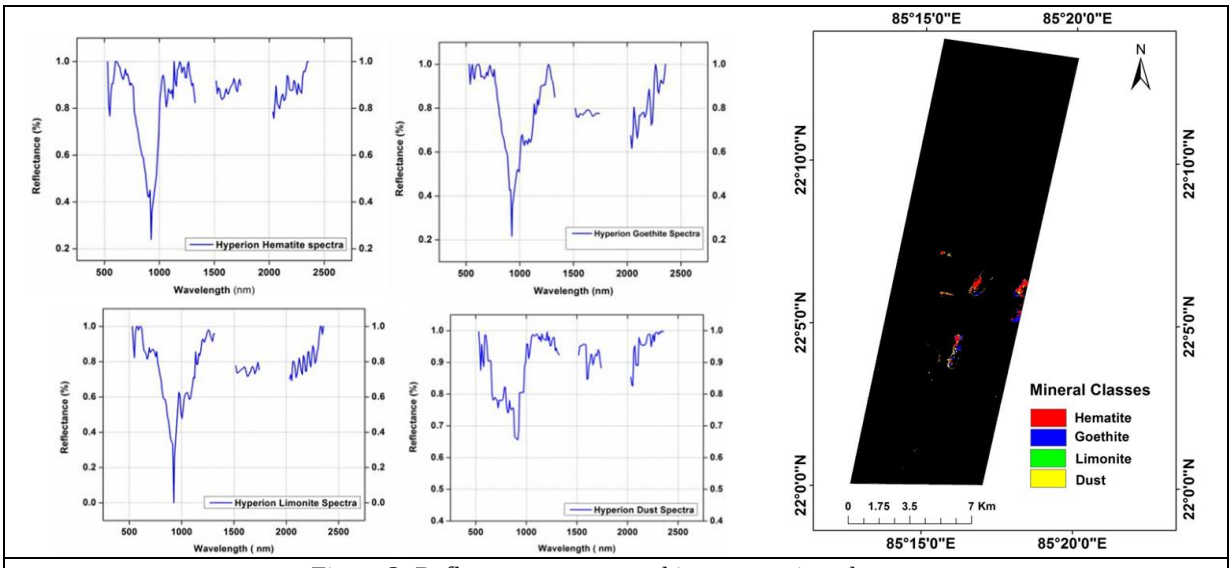

Figure 3: Reflectance spectra and iron ores minerals map

5.2 Results of abundance of endmembers:

Spectral unmixing (SU) allows the accurate identification and characterization of the materials found in the observed scene. For this given image, using a spectral unmixing method which aims at extracting the signatures of the different involved materials (called "endmembers"). It also estimates the relative proportions (called "fractional abundances") in each pixel of the image allowing a refined understanding of the scene. The real world is a complex mixture of different materials. Thus the depth of a material absorption is related to the abundance of the absorber and the grain size of the material. As mentioned that the strength of the iron absorptions depends on grain size. Larger grain sizes show the increased saturation of the 0.9-µm absorption and

broadening and shifting the apparent reflectance minimum to longer wavelengths. A continuum removal algorithm has been used to put them on a level and to retrieve the depth of the absorption feature. The mixing model has been used based on linear interaction abundance model. Here the abundances were interpreted as percentage and the sum of the abundance is equals to 1.In this study the classification image has been superimposed with Geology map for validation (Figure-4).

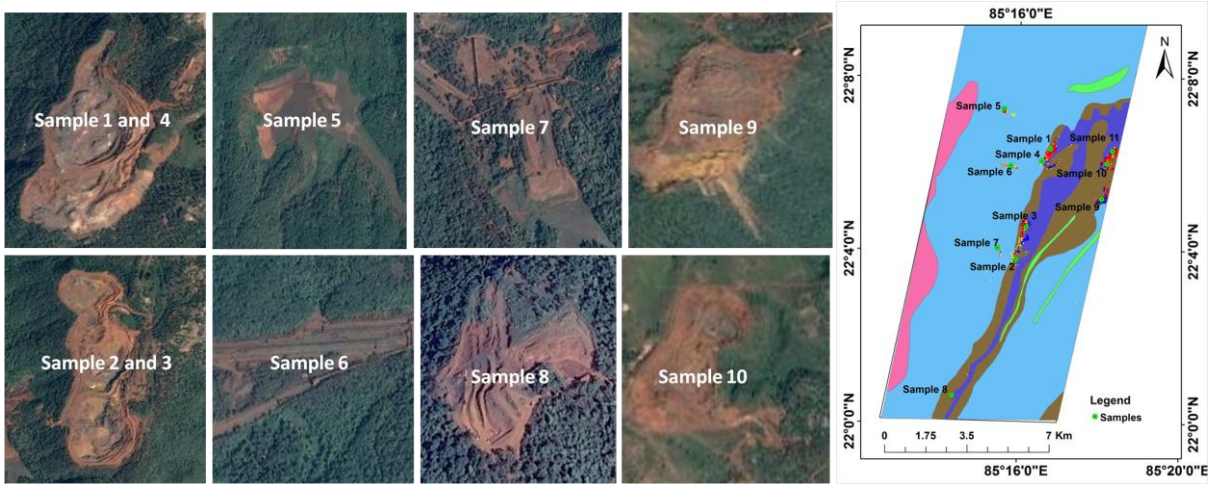

Figure: 4. Collecting different samples around the mines and showing the samples location in geological map

Here the Sample 1, 2, 3 has been collected from the Kiriburu and Meghahataburu iron ore mines where the Sample 1 predicts the large abundance of Hematite 70 % followed by Goethite 20 %, Limonite 5 % and Dust 5%. Where as the Sample 2 extracts the large abundance of Goethite of 75 % followed by Hematite and Limonite 10 % and Dust 5%. Sample 3 shows the Limonite concentration of 55 %, Hematite 38 %, Goethite 5 % and Dust 2 % (Figure-5). The rest of the sample has been collected from the out nearby side of the mines or the mineral flash out areas. These optimum mutual abundances were estimated by matching the computed mixed spectra signature with the FWHM of high-pass filtered Hyperion spectra while maintaining standard deviation of the error to a minimum value.

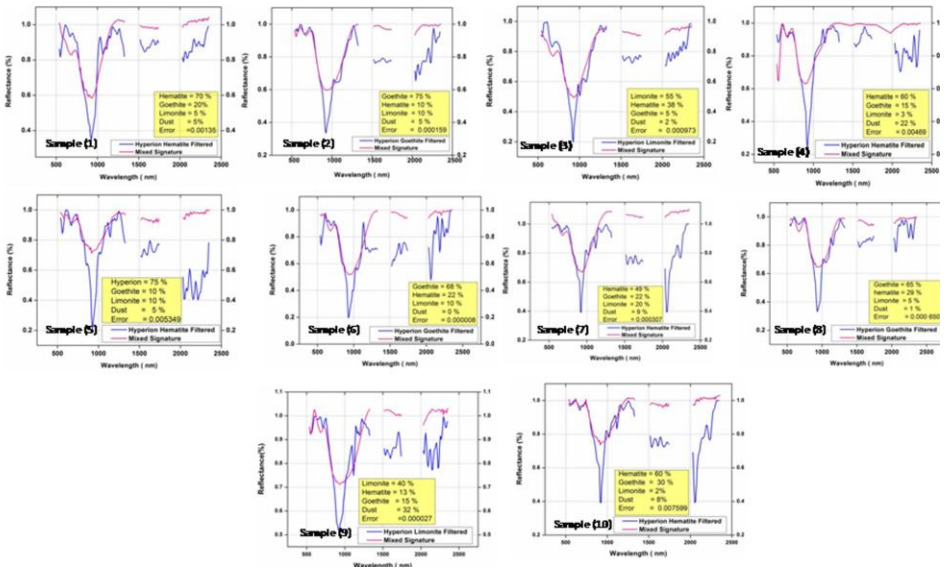

Figure: 5 Abundance of iron ore minerals in different samples

Discussion:

All minerals of the surface have its different physical and chemical properties. Therefore, different mineral has different absorption features on a particular wavelength range. The Kiriburu and Meghahataburu mines have the abundance of different mineral recourses. Kiriribiru is one of the most important Iron ore mining areas of Steel Authority of India Limited (SAIL). Banded Hematite Quartzite (BHQ) is the predominant iron ore in this region. The geological map indicates that other minerals

present include goethite, limonite and Blue Dusts. All these minerals have their own characteristic reflectance which when detected by hyperion sensor provides contiguous spectrum to identify or classify different mineral zone. Using the purest pixel of the n –dimensional visualizer or SAM algorithm method this area has been classified into the four iron ore mineral types as mentioned above i.e. Hematite, Goethite, Limonite and Blue Dust. The results indicate that the distribution of minerals on the surface is predominantly Hematite (36.7 %). This is followed by Goethite (32.05 %), Blue Dust (26.21 %) and Limonite (5.04). Number of other minerals are also present in the study area (As per UNCF), however, in those could not be matched with the available USGS spectrum. The spatial resolution of hyperspectral data is 30 m. It is more likely that more than one material contributes an individual spectrum measured by the sensor. Although the real world is a complex mixture of materials. In general, there are four types of mixtures: Linear Mixture: The materials in the field of view are optically separated so there is no multiple scattering between components. The combined signal is simply the sum of the fractional area times the spectrum of each component. This is also called aerial mixture. Intimate Mixture: An intimate mixture occurs when different materials are in intimate contact in a scattering surface, such as the mineral grains in a soil or rock. Depending on the optical properties of each component, the resulting signal is a highly non-linear combination of the end- member spectra. Coatings: Coatings occur when one material coats another. Each coating is a scattering/transmitting layer whose optical thickness varies with material properties and wavelength. Molecular Mixtures: Molecular mixtures occur on a molecular level, such as two liquids, or a liquid and a solid mixed together. Examples: water adsorbed onto a mineral; gasoline spilled onto a soil. The close contact of the mixture components can cause band shifts in the adsorb ate, such as the interlayer water in montmorillonite, or the water in plants. Using spectral unmixing method to estimate the abundance of endmember in a pixel. Computations for endmember abundances were done on spread sheet. Optimum mutual abundances were estimated by matching the computed mixed spectra signature with the FWHM of high-pass filtered Hyperion spectrum. In final result the spectrum of sample 1 concentrates the 70 % of Hematite which was collected from Kiriburu mines. Where in Sample 2 Goethite encompasses the highest concentration (75 %) of that spectrum. Where Limonite shows 55 % concentration and rest of the percentage has mixing of the the 3 minerals. It is to be noted that the filtered spectra and mixed spectra did not matched exactly because of the presence of other mineral. The classification and the ore characterization has been validate with the Geology and USGS library spectra because of the unavailability of Spectroradiometer.

Conclusion:

Remote Sensing Technology developing in India rapidly which has led to integration of this tool with different other fields. In this project the contiguous and narrow spectrum of hyperspectral data ranges from 400-2500 nm is ideal for discriminating and identifying minerals where the main absorption range of iron is 800-900 nm. Spectral variability is a phenomenon due, to a grand extends, to variations in the illumination and atmospheric conditions within a hyperspectral image, causing the spectral signature of a material to vary within a image. Data spectral fluctuation due to spectral variability compromises the linear mixing model (LMM) sum-to-one constraint, and is an important source of error in hyperspectral image analysis. Recently, spectral variability has raised more attention and some techniques have been proposed to address this issue, i.e. spectral bundles Endmember variability has been identified as one of the main limitations of the usual Linear Mixing Model, conventionally used to perform spectral unmixing of hyperspectral data. The topic is currently receiving a lot of attention from the community, and many new algorithms have recently been developed to model this variability and take it into account.

References:

Cloutis, E. A. (1996). Review article hyperspectral geological remote sensing: evaluation of analytical techniques. International Journal of Remote Sensing, 17(12), 2215-2242.

Crosta, A. P., Sabine, C., & Taranik, J. V. (1998). Hydrothermal alteration mapping at Bodie, California, using AVIRIS hyperspectral data. Remote Sensing of Environment, 65(3), 309-319.

Pournamdari, M., Hashim, M., & Pour, A. B. (2014). Spectral transformation of ASTER and Landsat TM bands for lithological mapping of Soghan ophiolite complex, south Iran. Advances in Space Research, 54(4), 694-709.

Ducart, D. F., Crósta, A. P., Souza Filho, C. R., & Coniglio, J. (2006). Alteration mineralogy at the Cerro La Mina epithermal prospect, Patagonia, Argentina: Field mapping, short-wave infrared spectroscopy, and ASTER images. Economic Geology, 101(5), 981-996.

Veganzones, M. A., Tochon, G., Dalla-Mura, M., Plaza, A. J., & Chanussot, J. (2014). Hyperspectral image segmentation using a new spectral unmixing-based binary partition tree representation. IEEE Transactions on Image Processing, 23(8), 3574-3589.

Halimi, A., Altmann, Y., Dobigeon, N., & Tourneret, J. Y. (2011). Nonlinear unmixing of hyperspectral images using a generalized bilinear model. IEEE Transactions on Geoscience and Remote Sensing, 49(11), 4153-4162.

Debba, P., Van Ruitenbeek, F. J. A., Van Der Meer, F. D., Carranza, E. J. M., & Stein, A. (2005). Optimal field sampling for targeting minerals using hyperspectral data. Remote Sensing of Environment, 99(4), 373-386.

Mendoza, C. (2002). Effect of genetically modified low phytic acid plants on mineral absorption. International journal of food science & technology, 37(7), 759-767.

Satpathy, R., Singh, V. K., Parveen, R., & Jeyaseelan, A. T. (2010). Spectral Analysis of Hyperion Data for Mapping the Spatial Variation of AL+ OH Minerals in a Part of Latehar & Gumla District, Jharkhand. Journal of Geographic Information System, 2(4), 210.

Kumar, C., Shetty, A., Raval, S., Champatiray, P. K., & Sharma, R. (2014). Sub-pixel mineral mapping using EO-1 Hyperion hyperspectral data. The International Archives of Photogrammetry, Remote Sensing and Spatial Information Sciences, 40(8), 455.

Magendran, T., & Sanjeevi, S. (2014). Hyperion image analysis and linear spectral unmixing to evaluate the grades of iron ores in parts of Noamundi, Eastern India. International Journal of Applied Earth Observation and Geoinformation, 26, 413-426.

Zadeh, M. H., Tangestani, M. H., Roldan, F. V., & Yusta, I. (2014). Sub-pixel mineral mapping of a porphyry copper belt using EO-1 Hyperion data. Advances in Space Research, 53(3), 440-451.

Pour, A. B., & Hashim, M. (2013). Fusing ASTER, ALI and Hyperion data for enhanced mineral mapping. International Journal of Image and Data Fusion, 4(2), 126-145.

Boardman, J. W., Kruse, F. A., & Green, R. O. (1995). Mapping target signatures via partial unmixing of AVIRIS data.

Bierwirth, P. N. (1990). Mineral mapping and vegetation removal via data-calibrated pixel unmixing, using multispectral images. International Journal of Remote Sensing, 11(11), 1999-2017.

Kruse, F. A., Lefkoff, A. B., & Dietz, J. B. (1993). Expert system-based mineral mapping in northern Death Valley, California/Nevada, using the airborne visible/infrared imaging spectrometer (AVIRIS). Remote Sensing of Environment, 44(2-3), 309-336.

Hubbard, B. E., & Crowley, J. K. (2005). Mineral mapping on the Chilean–Bolivian Altiplano using co-orbital ALI, ASTER and Hyperion imagery: Data dimensionality issues and solutions. Remote Sensing of Environment, 99(1), 173-186.

Bryant, R. G. (1996). Validated linear mixture modelling of Landsat TM data for mapping evaporite minerals on a playa surface: methods and applications. International Journal of Remote Sensing, 17(2), 315-330.

Drake, N. A., Mackin, S., & Settle, J. J. (1999). Mapping vegetation, soils, and geology in semiarid shrublands using spectral matching and mixture modeling of SWIR AVIRIS imagery. Remote Sensing of Environment, 68(1), 12-25.

Vaughan, R. G., Calvin, W. M., & Taranik, J. V. (2003). SEBASS hyperspectral thermal infrared data: surface emissivity measurement and mineral mapping. Remote Sensing of Environment, 85(1), 48-63.

Kayet, N., Pathak, K., Chakrabarty, A., & Sahoo, S. (2016). Spatial impact of land use/land cover change on surface temperature distribution in Saranda Forest, Jharkhand. Modeling Earth Systems and Environment, 2(3), 1-10.

Kayet, N., & Pathak, K. (2015). Remote sensing and GIS based land use/land cover change detection mapping in Saranda Forest, Jharkhand, India. Int Res J Earth Sci, 3(10), 1-6.

Sahoo, S., Dhar, A., Kayet, N., & Kar, A. (2017). Detecting water stress scenario by land use/land cover changes in an agricultural command area. Spatial Information Research, 25(1), 11-21.

Kayet, N., Pathak, K., Chakrabarty, A., & Sahoo, S. (2016). Urban heat island explored by co-relationship between land surface temperature vs multiple vegetation indices. Spatial Information Research, 24(5), 515-529.

Kayet, N., & Chakrabarty,(2016) A. Hyper spectral Image processing for Forest types Mapping and forest health monitoring: A case study in the buffer zones of iron mining belts of Saranda forest, Jharkhand, India.

Debba, P., Van Ruitenbeek, F. J. A., Van Der Meer, F. D., Carranza, E. J. M., & Stein, A. (2005). Optimal field sampling for targeting minerals using hyperspectral data. Remote Sensing of Environment, 99(4), 373-386.

Chen, X., Warner, T. A., & Campagna, D. J. (2007). Integrating visible, near-infrared and short-wave infrared hyperspectral and multispectral thermal imagery for geological mapping at Cuprite, Nevada. Remote Sensing of Environment, 110(3), 344-356.

Sanjeevi, S. (2008). Targeting limestone and bauxite deposits in Southern India by spectral unmixing of hyperspectral image data. The International Archives of the Photogrammetry, Remote Sensing and Spatial Information Sciences, 37(B8), 1189-1194.

Guha, A., Singh, V. K., Parveen, R., Kumar, K. V., Jeyaseelan, A. T., & Rao, E. D. (2013). Analysis of ASTER data for mapping bauxite rich pockets within high altitude lateritic bauxite, Jharkhand, India. International Journal of Applied Earth Observation and Geoinformation, 21, 184-194.

Gabr, S., Ghulam, A., & Kusky, T. (2010). Detecting areas of high-potential gold mineralization using ASTER data. Ore Geology Reviews, 38(1), 59-69.

Haest, M., Cudahy, T., Rodger, A., Laukamp, C., Martens, E., & Caccetta, M. (2013). Unmixing the effects of vegetation in airborne hyperspectral mineral maps over the Rocklea Dome iron-rich palaeochannel system (Western Australia). Remote Sensing of Environment, 129, 17-31.

Pour, A. B., & Hashim, M. (2014). ASTER, ALI and Hyperion sensors data for lithological mapping and ore minerals exploration. Springerplus, 3(1), 130.